Materials Science & Engineering A 814 (2021) 141195

Contents lists available at ScienceDirect

Materials Science & Engineering A

journal homepage: http://www.elsevier.com/locate/msea

Effect of solution annealing and precipitation hardening at 250 °C–550 °C on microstructure and mechanical properties of additively manufactured 1.2709 maraging steel

Ludmila Kučerová *, Karolina Burdová, Štěpán Jeníček, Iveta Chena

University of West Bohemia in Pilsen, RTI, Univerzitní 8, 301 00, Pilsen, Czech Republic

ARTICLE INFO

Keywords:
Maraging steel
Additive manufacturing
Selective laser melting
Solution annealing
Precipitation hardening

ABSTRACT

Post-processing heat treatment of additively manufactured (AM) maraging steel is an important issue in the tailoring of the final mechanical properties of a product. Up to now, mainly precipitation hardening at temperatures of 450 °C–500 °C has been studied either in as-built or solution-annealed samples. This work, however, presents an overview of the effect of much broader tempering temperatures of 250 °C–550 °C on the microstructure and mechanical properties of as-built maraging steel. Furthermore, the effect of previous solution annealing of AM steel at a lower temperature of 820 °C and at a higher temperature of 940 °C on subsequent precipitation hardening is also described. The results obtained for the precipitation behaviour of AM maraging steel are compared with those of conventionally produced maraging steel. The microstructure and mechanical properties of AM samples pre-annealed at 940 °C and precipitation hardened were found to be comparable to the conventionally processed reference sample at all hardening temperatures. On the other hand, the microstructures and properties of AM samples pre-annealed at 820 °C and precipitation hardened strongly resembled the results of as-built samples. However, even after a 6-h hold at the highest tempering temperature of 550 °C, distinct differences could still be found in the samples prepared with various initial conditions.

1. Introduction

Maraging steels are widely used in high-performance military, aerospace, automobile, tool and die applications [1–8]. They are used for engine casings and landing gear, products with conformal cooling channels, shafts, and fasteners. Furthermore, maraging steels are successfully used in tooling, as moulds for plastic injection and tools for die casting magnesium, zinc or aluminium alloys [9,10]. These applications are enabled by their suitable properties, mainly good toughness, and high resistance to crack propagation and thermal fatigue [9]. Maraging steels can also be used in structural parts which further require high resistance against high-cycle mechanical fatigue [11], combined stress and corrosion load [12], wear, and thermal fatigue [13]. When compared to H13 tool steel, which is also used for additive manufacturing, maraging steels possess better dimensional stability during ageing and a lower tendency to cracking during AM. Higher elastic modulus, lower thermal expansion along with good thermal conductivity reduce the surface temperatures under thermal loads, which results in lower thermal stresses [13,14].

The excellent combination of strength and toughness of maraging steels is due to the presence of nanoprecipitates within a ductile martensite matrix [9–23]. With their low carbon content (commonly below 0.03%), maraging steels develop a very ductile nickel-containing lath martensite upon solution treatment. Higher strength of the steel is provided by the subsequent aging treatment of this martensite, which enables intensive precipitation of the fine intermetallic particles [7]. The main strengthening mechanism which operates in maraging steels during ageing heat treatment is the precipitation of intermetallic phases such as Fe_2Mo, Fe_7Mo_6, Ni_3Ti and NiAl. It provides a tensile strength above 1500 MPa [24–31]. Dislocation looping [25,26] and shearing [32] were found to be the main phenomena in precipitation strengthening. In many maraging steels, longer ageing times or higher ageing temperatures also lead to reverted austenite formation, either alone or along with the intermetallics. If over-ageing occurs, strength, ductility, and toughness decrease. However, there have been reports of improved toughness due to the reverted austenite [33].

Many researchers have conducted in-depth investigations into the precipitation behaviour and the analysis of the strengthening

* Corresponding author.
E-mail addresses: skalova.lida@seznam.cz, skal@rti.zcu.cz (L. Kučerová).

https://doi.org/10.1016/j.msea.2021.141195
Received 11 December 2020; Received in revised form 20 March 2021; Accepted 29 March 2021
Available online 2 April 2021

mechanism triggered by the aging treatment after solution annealing [9, 17–22]. However, earlier studies were only concerned with conventionally produced maraging steels. By contrast, those involving additively-manufactured (AM) steel focused on heat treatment around the recommended temperatures of 450 °C–500 °C. Very little attention has been paid to the effect of lower hardening temperatures or to the comparison between precipitation-hardened AM steel and solution-annealed and precipitation-hardened AM steel.

The aim of this study was therefore to evaluate the effect of precipitation hardening on the mechanical properties and microstructure of additively-manufactured MS1 steel with respect to previous solution annealing. It was assumed that various conditions of AM steel prior to precipitation hardening might impact the phase transformation during the hardening process and therefore the resulting mechanical properties. An extensive heat treatment experiment was designed to study this impact and to provide processing windows for the desired combinations of mechanical properties. In practice, AM steels are typically required to possess mechanical properties close to (or perhaps better than) those of the equivalent conventional steel. Therefore, the same precipitation treatment schedules were applied to both AM steel and a conventionally processed reference steel.

Furthermore, isothermal holding at lower temperatures for various times may be also relevant from the application viewpoint. Parts made from the steel may experience expected or unexpected temperature exposure in service. It is therefore useful to know the effects of thermal exposure on the stability of its microstructure and mechanical properties.

2. Experiment

2.1. Materials

Maraging tool steel designated 1.2709 was supplied in the form of a powder under the trade name MS1 by EOS and in the form of conventionally-manufactured Vaco 180 from Bohdan Bolzano, s.r.o. (Table 1). The maraging steel is equivalent to 18Ni-300 grade and X3NiCoMoTi 18-9-5 grade. The powder was produced by gas atomization which leads to relatively spherical particles. The conventionally manufactured steel had been warm rolled to a cross section of 250 × 250 mm and a length of 1000 mm and solution-annealed state (820 °C/1 h) by the supplier. The delivered bar was then finally cut into 40 mm long samples with a square cross section of 10 × 10 mm for subsequent heat treatment. The initial microstructure of the conventionally manufactured steel consisted of lath martensite.

2.2. Additive manufacturing

All the AM samples were built as cylinders with 9 mm diameter and 75 mm height, using the same processing parameters, in the EOS M290 machine in a nitrogen atmosphere. The growth direction of the samples was oriented in the z-direction, i.e. the axis of the cylinder was perpendicular to the base plate. The cores of all the samples were produced using processing parameters that are recommended for tool steels, a laser power of 258 W, a scanning rate of 960 mm/s, a layer thickness of 40 μm, hatch spacing of 110 μm and a misorientation angle of 67°. The contour (the whole surface) of each sample was deposited using different processing parameters with a scanning rate of 300 mm/s and a laser power of 138 W.

2.3. Heat treatment

The same precipitation treatment schedules were applied to both MS1 and conventionally processed Vaco 180 reference steel. Precipitation treatment was performed on MS1 in three different conditions: as-built, solution-annealed at 820 °C for 60 min, and solution annealed at 940 °C for 120 min. The latter two conditions were based on the obsolete (820 °C/60 min) and the new (940 °C/120 min) recommendations from the powder supplier. After solution annealing, the specimens were cooled in a furnace. The conventionally manufactured Vaco 180 steel was precipitation-treated in the as-delivered condition (warm rolled and solution-annealed). All heat treatments were performed under an argon atmosphere.

The precipitation treatment involved heating to temperatures in the range of 250 °C–550 °C and holding for 0–6 h. The actual temperature of the samples was measured using a thermocouple placed in a hole drilled in the centre of one of the samples. After precipitation treatment, the samples cooled in air. Where the hold is identified as “0”, the samples were merely brought to the temperature and once the desired temperature was reached according to the inserted thermocouple, the samples were left to cool at ambient air temperature.

2.4. Characterisation

Tensile properties of all samples were tested using sub-size flat test pieces (Fig. 1). They were produced from the bulk AM and conventional material by wire cutting and subsequent grinding to a final thickness of 1.2 mm. All tensile samples were cut from the central part of the heat-treated samples, along the building direction in the case of AM steel and along the rolling direction in the case of the conventional reference steel Vaco 180. The samples had a gauge length of 5 mm and a width of 2 mm. A Zwick Roell Z250 testing machine was used for mechanical testing, following EN ISO 6892–1. A constant strain rate of 0.0067 s^{-1} was applied to all tested samples. Hardness (HV10) of the four initial conditions was measured on the top section of the AM samples and on the transverse cross-section through a conventionally produced VACO 180 bar, using a Wolpert 432-SVD instrument and 10 kg load and 10 s dwell.

The microstructures of all the samples were investigated by light microscopy and scanning electron microscopy (SEM) with energy-dispersive X-ray spectroscopy (EDS) and electron back-scattered diffraction (EBSD) detectors. The grain tolerance angle of 2° was used and the transition angle between sub-grains and grains was set to 10° for evaluation of EBSD results. EBSD was used on the metallographic

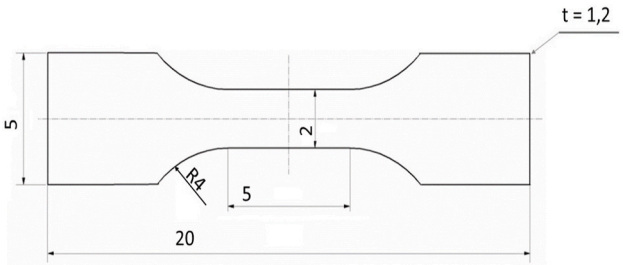

Fig. 1. Sub-size flat specimen for tensile test (dimensions of the sample given in mm).

Table 1
Chemical composition of both forms of the steel and reference values from the material data sheet in weight %.

	C	Si	Mn	Cr	Mo	Ni	Co	Ti	Al
Data sheet	≤0.03	≤0.1	≤0.1	≤0.5	4.5–5.2	17–19	8.5–9.5	0.6–0.8	0.05–0.15
MS1	0.001	0.02	0.02	–	4.9	17.7	8.7	0.8	0.06
Vaco 180	0.003	0.02	0.06	0.12	4.8	18.2	8.8	0.8	0.06

sections of the powder and also on samples treated with the lowest and the highest precipitation temperatures. However, more detailed EBSD observation was performed only on samples where X-ray diffraction determined the highest contents of reverted austenite. These methods were limited in their ability to identify fine particles. These particles were not numerous enough to be detected by X-ray analysis, whereas only the coarse ones were suitable for EDS examination. A spark optical emission spectrometer Tasman Q4 was used to determine the chemical composition of the bulk AM material. Five measurements were carried out at freshly grinded surface of the AM steel.

Metallographic samples referred to as 'side cross-section' were prepared along the building direction. The top cross-section was parallel to the hatching planes (Fig. 2). The microstructures were observed in a Crossbeam Auriga Zeiss scanning electron microscope with high resolution and a field emission gun and a BX61 Olympus light microscope. The sections from AM steel, conventionally processed steel and the powders were prepared in the standard way by mounting, mechanical grinding and polishing, using diamond polishing suspensions (9 μm, 3 μm and 1 μm). The samples determined for EBSD analysis were further polished by OPS colloidal silica suspension. Etching with 3% Nital and diluted aqua regia (H_2O:HNO_3:HCl = 6:1:3) was used to reveal the microstructures. Powder particle sizes were evaluated by image analysis of SEM micrographs taken at 1000× magnification. The diameters of 250 particles were measured.

The substructure of the as-built sample was observed by transmission electron microscopy (TEM) of thin foils using the JEOL 200 CX with the accelerating voltage of 200 kV. The foils were prepared from the discs with the original thickness of 1.5 mm which were mechanically grinded from both sides using papers (600 and 1200) to the thickness of 80–100 μm. Small discs of the diameter of 3 mm were cut out from these thinned samples. The final thinning was carried out in Tenupol 5 in an electrolyte consisting of 300 ml HNO_3 a 700 ml CH_3OH, at the 15 V and −10 °C.

The volume fraction of phases was measured and analysed using an X'Pert Pro PANalytical powder diffractometer with a Co Kα X-ray doublet radiation and an X'Celerator position-sensitive detector. The patterns were obtained using Bragg-Brentano geometry and further processed by X'Pert HighScore Plus software to identify the phases. Rietveld refinement using Topas V3 software was subsequently carried out to provide the weight ratios of the present phases.

The porosity of the AM steel was evaluated by image analysis of top and side cross sections. AM sample was cut longitudinally in half and one part was analysed in an as-built condition while the other part was solution annealed at 940 °C for 2 h before the analysis. Top and side cross sections were prepared from the same positions in as-built and heat-treated part. This approach was chosen to eliminate the effect of printing parameters, position at the platform, distance above the platform, distribution of surrounding parts, etc. on the porosity of evaluated parts. In both cases, analysed area in top and side cross sections always consisted of 10 × 10 images obtained by the 50× magnification lens using laser scanning confocal microscope Olympus LEXT OLS 5000. Stitched images of the whole area were then processed by the image analysis software Olympus Stream and the plane fraction of the defects was evaluated. To assess the homogeneity of pore distribution, all the samples were roughly grinded after the first analysis, fine grinded and polished and the second set of measurements was carried out in the same way but in the location about 1 mm below the originally evaluated surface.

3. Results

3.1. Powder

The average particle diameter of the powder was 25 μm. The size distribution graph (Fig. 3) shows that most particles were within the 20–30 μm size range. A metallographic section was prepared from a representative sample of the virgin powder.

The powder was examined using EBSD. The presence of retained austenite (shown in blue in Fig. 4) at cell boundaries was revealed. It is related to a rather strong segregation of alloying elements, namely Co, Mo and Ti, at cell boundaries, which supports austenite stabilization.

3.2. Microstructure analysis

Observation using an optical microscope did not yield sufficient information about the microstructures. Therefore, an extensive examination using SEM was performed and accompanied by EBSD characterisation. EBSD was also used to confirm the presence of retained and reverted austenite. X-ray diffraction phase analysis was employed to estimate the volume fraction of austenite in the microstructure. Even though the number of fine precipitates can be expected to rise with increasing hardening temperature and time, their presence was not confirmed by the X-ray measurement, as their volume fraction remained below the detection limit of the method. In addition, the precipitates were too fine to be examined using standard SEM or EBSD. A separate study will, therefore, be dedicated solely to TEM observation of precipitates which are formed during hardening at various temperatures.

3.2.1. Electron microscopy

Light microscopy could not provide enough information about the microstructure, as AM steels have generally very fine cellular structures which become indistinct in light micrographs [16]. Transmission electron microscopy was used to show the substructure of the as-built AM steel (Fig. 5) and scanning electron microscopy was then employed (Fig. 6, Fig. 7, Fig. 8), along with EDS analysis of the local chemical composition of the particles, and EBSD (Fig. 9, Fig. 10) to characterise the microstructures. The process of precipitation in this AM steel has been relatively well documented by researchers using high resolution imaging methods, such as atom probe tomography or HRTEM, even though there is some disagreement concerning the exact stoichiometry of the particles. Little work has been done so far on the detailed

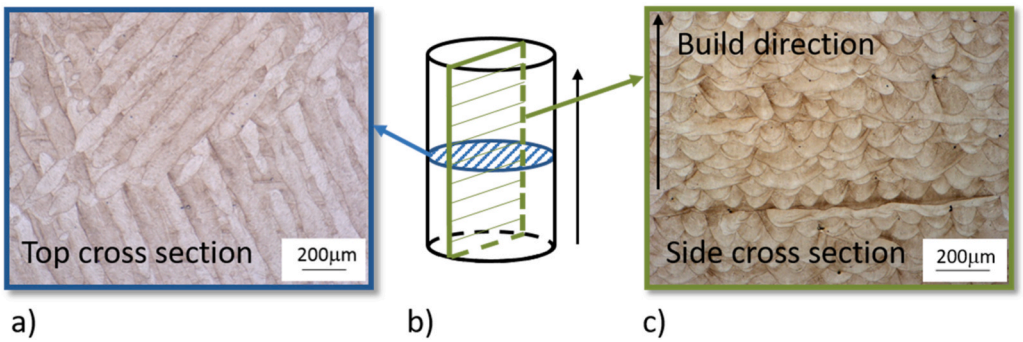

Fig. 2. The position of metallographic sections within the sample b) with light micrographs of a) top section and c) side section.

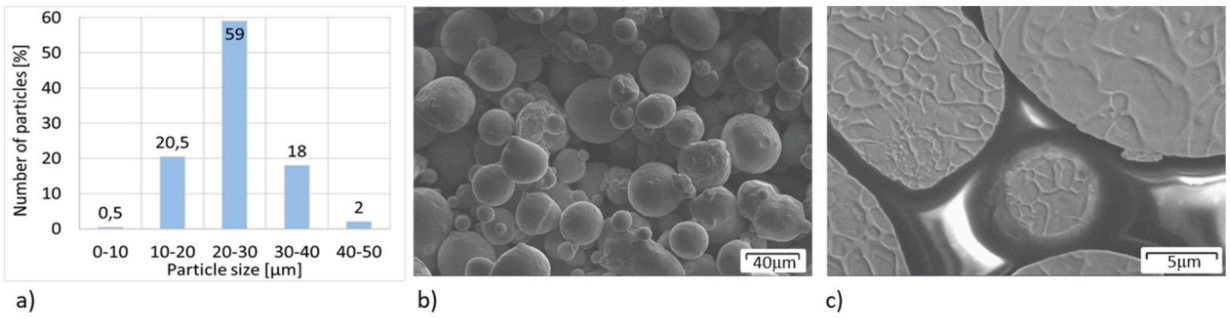

Fig. 3. Analysis of the powder: a) particle size distribution, b) detail of powder particles, c) metallographic section of powder.

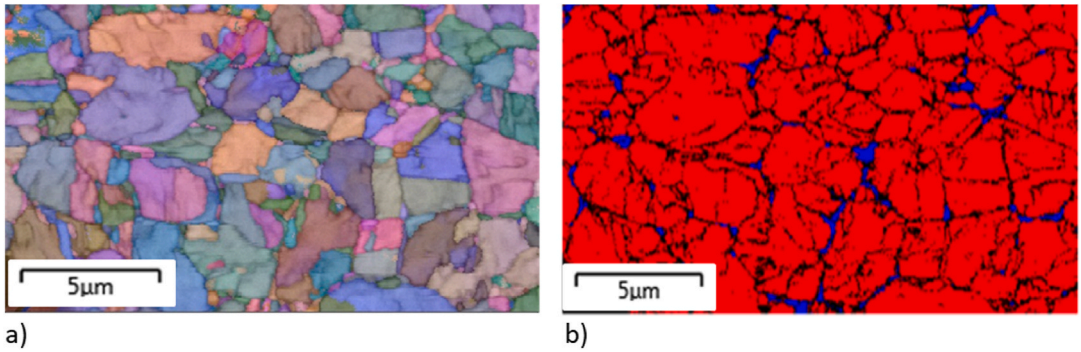

Fig. 4. Results of EBSD analysis: a) Euler map, b) phase fraction with austenite in blue and ferrite in red. (For interpretation of the references to colour in this figure legend, the reader is referred to the Web version of this article.)

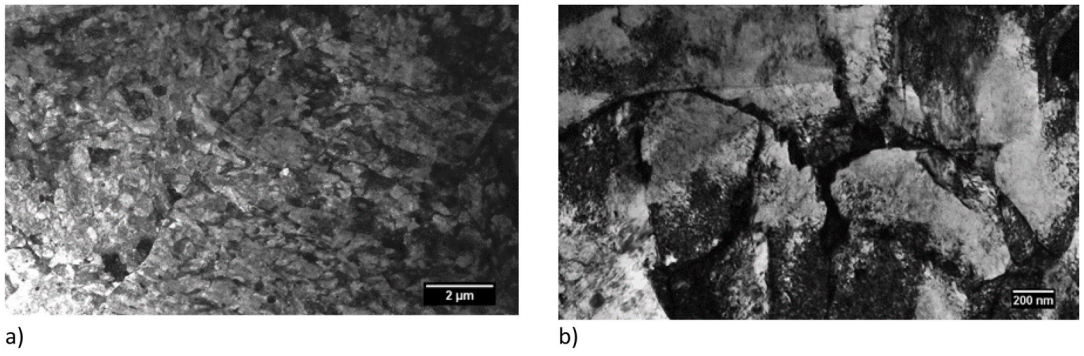

Fig. 5. TEM images of the substructure of as-built sample, a) overview with fine polyhedral grains with high dislocation density and particles of irregular shape at their boundaries, b) detail of polyhedral grains with higher dislocation density and smaller grains of irregular shape at their boundaries.

microscopic characterisation of AM steel after solution annealing. That having been said, based on earlier differential scanning analysis (DSC) measurement, the ageing sequences and austenite reversion are expected to be equivalent in precipitation-hardened AM maraging steel and solution-annealed and precipitation-hardened AM steel [34].

The microstructure of the as-built AM samples was cellular with very fine particles and about three percent of retained austenite. While the cell boundaries are well-formed in SEM micrographs, there are no laths or other microstructure features visible inside of the cells. The substructure of the AM steel is apparent only from the TEM micrographs which show fine, mainly polyhedral grains with various dislocation density. Areas with high dislocation density are typically found in as-built AM maraging steel.

AM samples were further found to contain very fine spherical particles with increased levels of titanium, aluminium and oxygen along with coarse Ti oxides, typically around 1 µm or larger. Large magnifications of 30 thousand times or more were necessary for documenting the fine globular particles (Fig. 6a), with the diameter typically around 40 nm. Line EDS analysis confirmed increased levels of Ti, Al and O in these particles (Fig. 6c). The line intersected a particle near the cell boundaries (marked by arrows in Fig. 6c). Finer particles were also observed in the as-built microstructure. However, it was impossible to determine their chemical composition by EDS. They might have been extremely fine Ni_3Ti precipitates or Ti oxides. Surprisingly, rare and very fine, sharp-edged particles (Fig. 6b, d) were also observed in the microstructure. EDS analysis identified increased contents of Al, Ti and N in these particles, which might result from nitrogen captured within the sample during AM processing in a nitrogen atmosphere. However, the average nitrogen content in the as-built part was below the detection limit of the spectrometer, which for nitrogen corresponds to 0.001 wt %.

The microstructures produced by low-temperature hardening of the AM as-built samples were very similar to the as-built microstructure. The microstructures obtained after 6 h at 250 °C (Fig. 7b) demonstrated this; they consisted of mixtures of equiaxed and elongated cells and

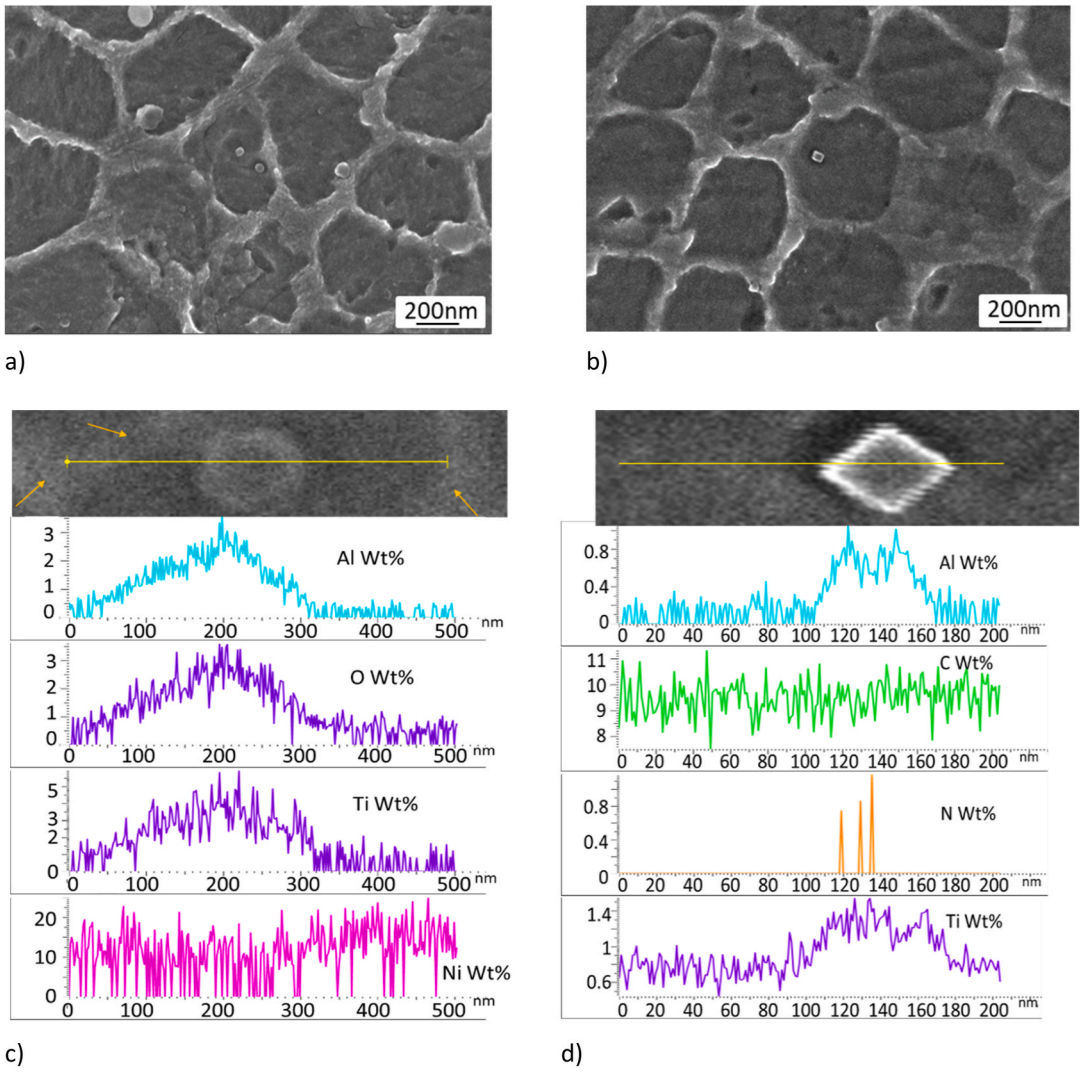

Fig. 6. Very fine particles in the as-built microstructure of maraging steel without subsequent heat treatment, with mainly globular particles a), and very rare sharp-edged particles b), and corresponding line EDS analysis across globular Ti–Al–O particle c), and sharp-edged Al-Tin-N particle d).

particles. Subsequently, with increasing hardening temperatures, cell boundaries first became discontinuous which started to be visible in micrographs from approximately 400 °C, as it was also confirmed in Ref. [16].

After long precipitation hardening times at 500 °C and 550 °C, parts of the original AM cell boundaries became thicker, as reverted austenite started to form and grow there. It has been reported that it is energetically favourable for reverted austenite to form Ni-enriched shells around existing retained austenite [6]. The cellular microstructure obtained in the as-built AM steel at this temperature is the finest of all the conditions which were examined (cf Fig. 7c, f, i, l).

The occurrence and size of particles gradually increased as the hardening temperature increased from 350 °C to 550 °C (Fig. 8). This corresponds to the increase of Ni_3Ti precipitates, previously reported by other authors to be visible with increasing hardening temperatures around 400 °C and higher [4], as the original precipitates coarsened and new particles formed and began growing. Besides the original Ni_3Ti and newly-formed Ni_3Ti particles, particles in which Ti was substituted by Mo or Al also emerged in the form of Ni_3Mo or Ni_3Al [6]. The needle-like particles of A_3B type creating networks and having preferential orientations were also found in over-aged samples annealed for 6 h at 550 °C (Fig. 7). Those rod or needle-like particles were observed also by other researchers in maraging steel hardened at or above 480 °C [7]. Local segregation of nickel was found in the samples over-aged for 6 h at 550 °C, suggesting the transformation of Ni_3Mo particles to the Fe–Mo based particles, previously identified as the equilibrium Fe_2Mo phase [4] or Fe_7Mo_6 phase [34].

A similar development to the as-built AM samples was seen in the AM samples which were solution-annealed at 820 °C. This heat treatment step removed some of the chemical heterogeneity and residual stresses induced by additive manufacturing. Only indistinct traces were found of the original cells of all morphologies. These results might be compared to the report of Conde et al. [33] that even after 1-h solution annealing at 820 °C, the microstructure still retained features typical of the as-built AM condition. Solution annealing of AM steel at 820 °C resulted in the dispersion of very fine precipitates within the matrix. They were previously identified by the authors mainly as Ni3Ti, Ni3(Ti, Mo) particles with a rare occurrence of particles with increased Co content, the detailed analysis was described in Ref. [16]. The particles were also found along grain boundaries. With the cell microstructure less pronounced, these very fine particles became more readily visible than in the micrographs of the as-built condition (Fig. 7b, e). A similar microstructure was found in the samples annealed at low temperatures, such as the one annealed for 6 h at 250 °C (Fig. 7e). Significant changes occurred at higher hardening temperatures, most notably after 6-h hardening at 550 °C. The original cell boundaries, which nearly

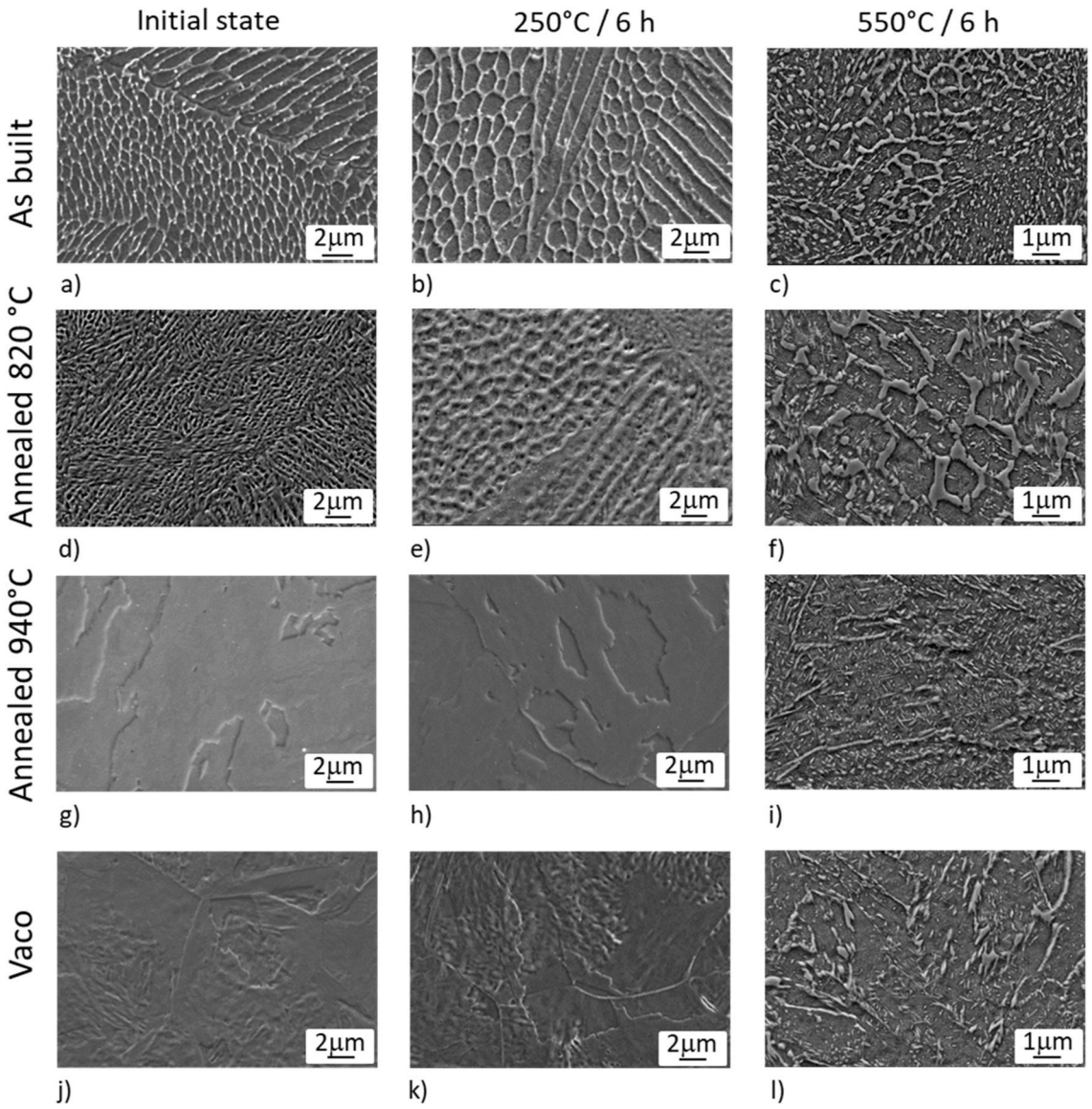

Fig. 7. Microstructure overview of the initial condition (a,d,g,j) and samples annealed for 6 h at 250 °C (b,e,h,k) and 550 °C (c,f,i,l).

vanished during pre-annealing at 820 °C, became clearly visible again, even though discontinuous, due to the preferential formation of reverted austenite in these areas (Fig. 7f).

AM samples pre-annealed at 940 °C showed no traces of the AM cell microstructure because long times at high temperature promoted the uniform distribution of the alloying elements, relieved most residual stresses and produced a typical lath microstructure after cooling (Fig. 7g). Significantly smaller amounts of very fine particles were found in the initial microstructure when compared to AM samples pre-annealed at 820 °C. While no distinctive differences were observed after low temperature hardening (Fig. 7h), very different microstructures were obtained with higher temperature hardening (Fig. 7i). Packet or lath boundaries became effectively invisible due to very intensive precipitation and austenite formation. Longer thin films and islands of austenite often formed along parts of the packet or lath boundaries and fine rod-like particles with preferential orientations were densely distributed in the matrix (Fig. 7i). This would be in line with Jagle's [6] description of A_3B type particles which formed oriented networks in over-aged samples. The comparison of all the initial conditions revealed that A_3B particles were most frequent in AM samples solution-annealed at 940 °C and hardened for 6 h at 550 °C.

Similar microstructure development as in the AM samples pre-annealed at 940 °C was observed in conventionally manufactured Vaco steel, where higher temperature hardening also resulted in a completely different microstructure (Fig. 7l) than for low temperature hardening (Fig. 7k). Similar patterns of thin elongated austenite islands at prior grain boundaries were accompanied by fine rod-like particles (Fig. 7l). The number of these fine particles was lower than in the case of AM samples pre-annealed at 940 °C and precipitation-hardened with the same procedure.

3.2.2. *EBSD*

Changes in the microstructure with increasing hardening temperature were further identified using EBSD (Figs. 9 and 10). Differences were also detected in the initial microstructures of the four materials. The black boundaries in the images indicate high-angle boundaries (i.e. grain boundaries). Low angle boundaries (i.e. sub-grain boundaries) are not marked in the micrographs in order to keep the images uncluttered. AM samples pre-annealed at 940 °C possessed a microstructure very similar to the conventionally manufactured Vaco, in terms of both morphology and size.

The microstructures of AM samples pre-annealed at 820 °C, on the

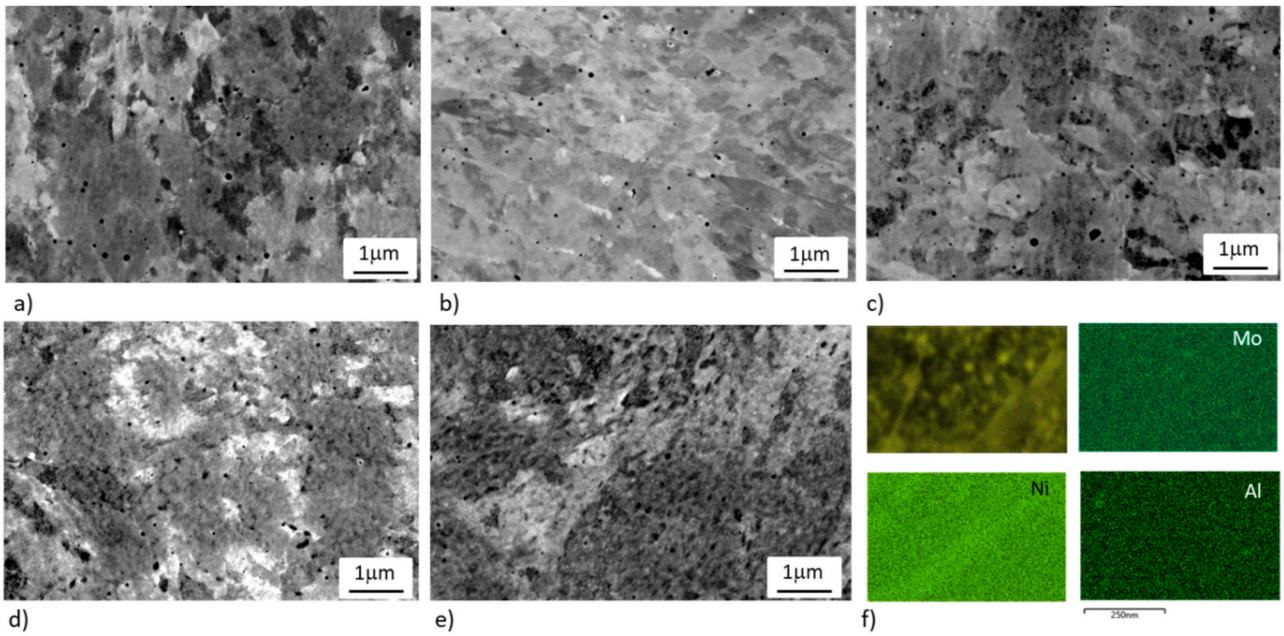

Fig. 8. Typical particle sizes and their distribution in AM samples a) AM as-built, b) AM hardened at 350 °C/6 h, c) AM hardened at 400 °C/6 h, d) AM hardened at 500 °C/6 h, e) AM hardened at 550 °C/6 h, f) details of element distribution in AM hardened at 550 °C/6 h. a)-e) samples were polished and observed by a BSE (backscattered electrons) detector.

other hand, were very much a finer version of the microstructures of the as-built AM samples. In the as-built samples, grains coarsened with increasing hardening temperatures. The initial very fine grains and subgrains coalesced to form larger areas with a similar crystallographic orientation. This was first observed on a smaller scale after 6 h at 250 °C. It was more extensive at higher precipitation hardening temperatures, eventually resulting in packets of elongated lath-like areas with a 20–40 µm length and different thicknesses after 6-h hardening at 550 °C. The smallest grains and subgrains disappeared after 6-h hardening at 250 °C but they reappeared after 6-h hardening at 550 °C. This appears to be related to an ongoing phase transformation – a reversion of the austenite in this process step where fine grains of austenite emerge.

The microstructures of AM samples pre-annealed at 820 °C showed a similar trend of coarsening at higher hardening temperatures. In this case, relatively thin and fine laths became more pronounced and prevailing in the microstructure with increasing hardening temperature.

Significant grain coarsening occurred in Vaco samples as well. There, individual coarse grains with large laths within, surrounded by smaller grains, were found after 6-h hardening at 250 °C. Furthermore, after 6-h hardening at 550 °C, the grains were generally larger than in the original condition and their size distribution was more heterogeneous than that after low-temperature hardening.

The distribution of austenite in the microstructures was easier to examine after precipitation hardening at higher temperatures (Fig. 10). The first reason was the small amount of austenite in the initial microstructures and after hardening at low temperatures. Besides, these austenite islands were rather fine, in the form of thin films along grain or cell boundaries. It was therefore very difficult to detect them using EBSD. Grain or cell boundaries are typically the most difficult regions to index in any EBSD map. Any fine particles of phases in these areas are easily lost as “zero solutions” (i.e. unidentified pixels). With the increasing total volume fraction of austenite and the size of its particles in the microstructure, the probability of detection by EBSD increases if reasonably high magnifications are used.

Fig. 10 shows that after hardening at 550 °C, retained and reverted austenite in the as-built sample was the easiest to detect. In this sample, the highest austenite volume fraction was also found by X-ray diffraction phase analysis.

3.2.3. *X-ray diffraction phase analysis*

According to X-ray diffraction measurement, the highest volume fraction of austenite was in the as-built samples, regardless of the precipitation hardening treatment (Fig. 11). It is certainly related to the presence of about 4% retained austenite in the as-built samples prior to any hardening [16]. This finding is in agreement with reports and publications on AM maraging steel [3,4,7]. It differs from conventionally manufactured maraging steel which is ordinarily delivered in a solution-annealed condition without any austenite. It should be noted that low amounts of austenite, i.e. several percent (below 5%), are close to the detection limit of the method and should be considered a rough estimate which confirms that some austenite is present, rather than an exact value. A significant increase in the austenite fraction occurred after 6-h hardening at 500 °C, except for the AM sample annealed at 940 °C. The austenite content in the as-built sample reached nearly 10%, which suggests that reverted austenite formed. For the precipitation hardening temperature of 550 °C, even the “0 h” holding time resulted in an appreciable increase in the austenite fraction in the as-built, AM annealed at 820 °C and Vaco samples. Austenite content increased dramatically with 6-h precipitation hardening at 550 °C: more than 30% austenite in the as-built sample, 23% in the AM sample pre-annealed at 820 °C, 15% in the AM sample pre-annealed at 940 °C, and 13% in Vaco. The original microstructure clearly had a profound influence on the transformation behaviour of the maraging steel. The as-built microstructure with the most heterogeneous distribution of alloying elements, which was obtained by additive manufacturing without subsequent solution annealing, had the largest amount of austenite. The reason is that the areas with higher solute levels are ideal nucleation sites for austenite transformation. This process can be traced to some extent in scanning electron micrographs.

3.2.4. *Porosity*

Porosity was tested by two sets of measurements for the AM sample in as-built condition and after solution annealing at 940 °C for 2 h. The analysis was always carried out at side and top cross sections. The second measurement was taken about 1 mm below the position of the first measurement. The plane fraction of the defects was established by image analysis of 100 images in each cross section (Table 2).

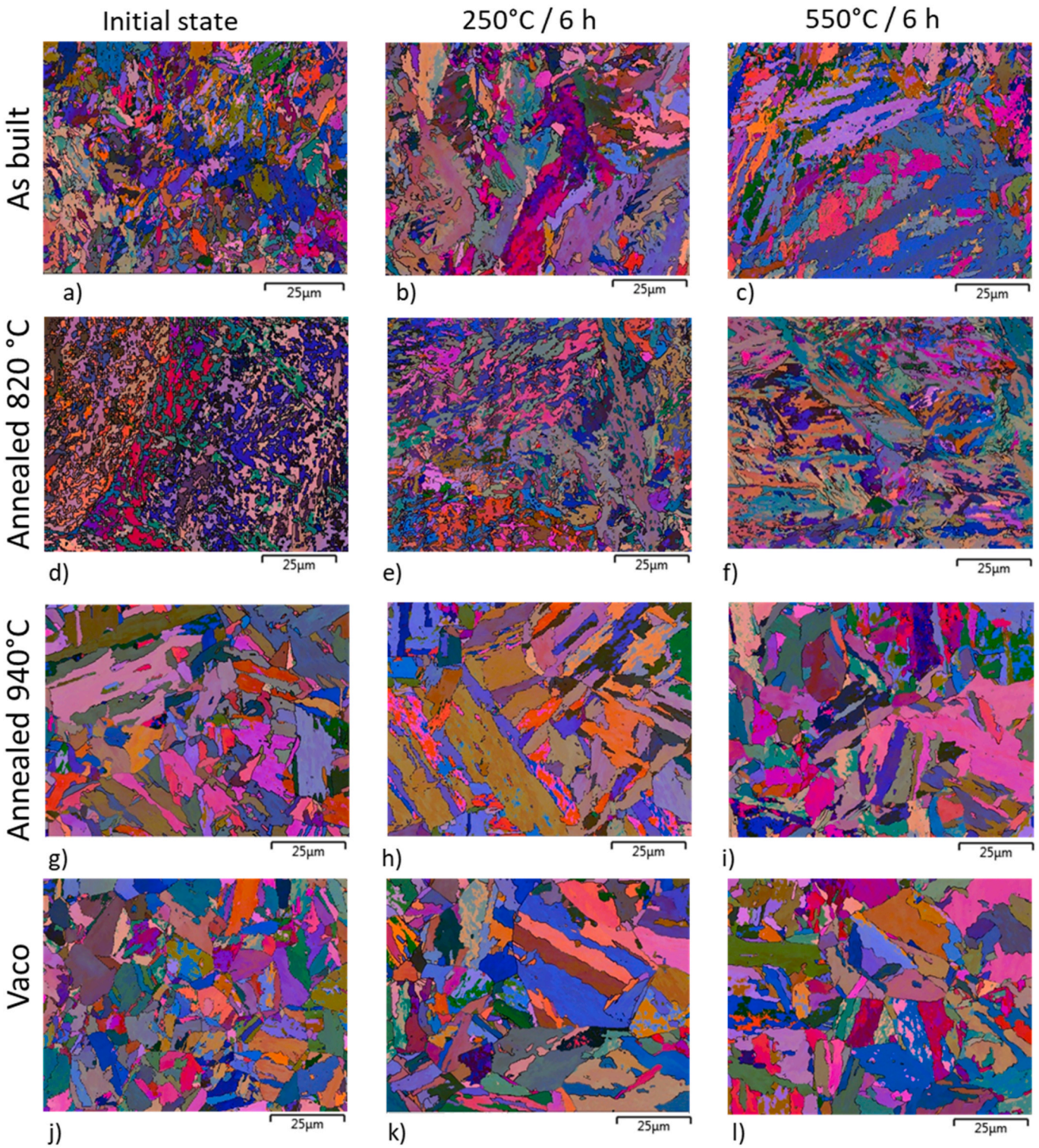

Fig. 9. EBSD overview (Euler maps) of the initial microstructures (a,d,g,j) and samples annealed for 6 h at 250 °C (b,e,h,k) and 550 °C (c,f,i,l).

The results show that the porosity could differ in various areas of the sample. And even though a relatively large amount of images were evaluated, comparative measurement carried out only in a single plane could provide misleading results. For example, the second measurement of 100 images would suggest that the solution annealing heat treatment significantly decreased the porosity of the AM steel in top cross section, from 0.22% to 0.05%. However, different pictures emerge from the comparison of the porosity values of both measurements and their average values. The average plane porosity of the sample after heat treatment was in both cross sections slightly higher than in the as-built condition. It suggests that the porosity is rather heterogeneously distributed within the AM sample and solution annealing does not seem to have any significant effect on porosity of the steel. A second conclusion of this experiment is that side cross sections tend to have lower porosity values than top cross sections. This difference was consistently observed for both conditions in both measurements.

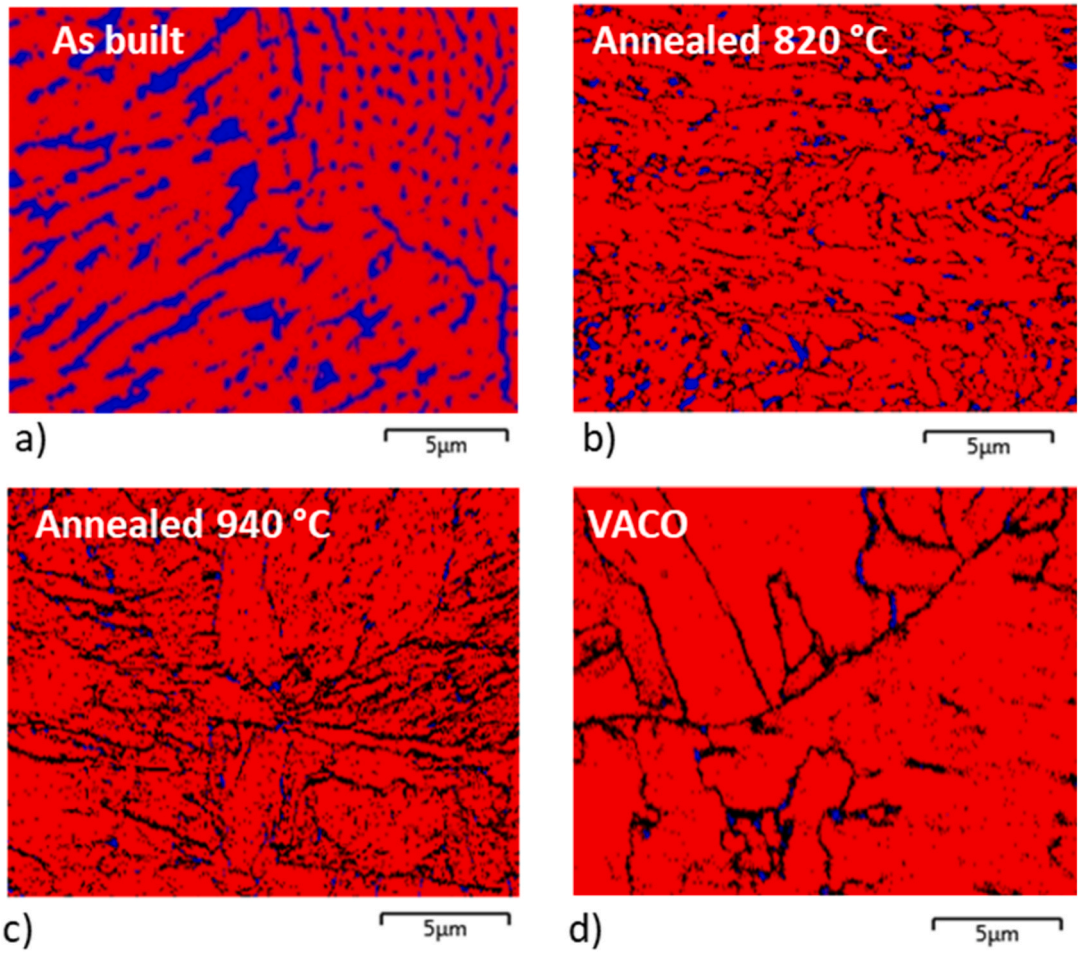

Fig. 10. Detailed EBSD phase maps of microstructures annealed for 6 h at 550 °C for all initial conditions: a) As-built, b) Annealed 820 °C, c) Annealed 940 °C, d) VACO. Blue – austenite, red – ferritic matrix. (For interpretation of the references to colour in this figure legend, the reader is referred to the Web version of this article.)

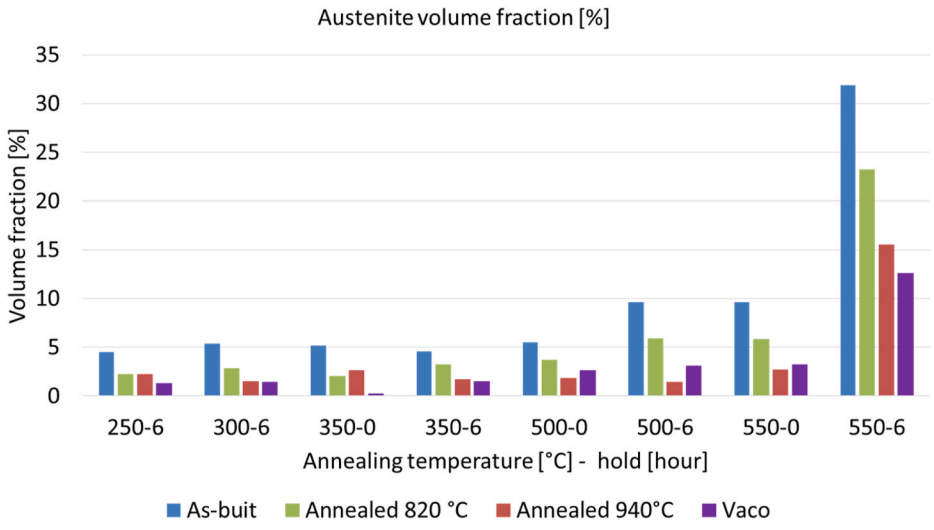

Fig. 11. Austenite volume fraction as established by X-ray diffraction phase analysis.

3.3. Mechanical properties

3.3.1. Mechanical properties in initial conditions

Mechanical properties of additively manufactured (AM) maraging steel in as-built and solution annealed conditions differ. Therefore, the properties of the four initial conditions of the material were determined first to be used as reference values (Table 3). Hardness (HV 10) was measured on the top cross-section of the AM samples and on the transverse cross-section through a conventionally produced Vaco bar. The AM steel without additional heat treatment (i.e. as-built) had the highest

Table 2
Plane fraction of defects in [%] determined by image analysis.

Condition	Sample	1. Porosity	2. Porosity	Average porosity
MS1-as built	Side cross section	0.11	0.15	0.13
	Top cross section	0.23	0.22	0.225
MS1-940°C-2 hours	Side cross section	0.19	0.13	0.16
	Top cross section	0.43	0.05	0.24

Table 3
Reference mechanical properties of the materials in their initial conditions, yield tensile strength (YTS), ultimate tensile strength (UTS), total elongation (TE), hardness (HV10).

Material and heat treatment	YTS [MPa]	UTS [MPa]	TE [%]	HV 10
AM as-built	815 ± 5	955 ± 7	19 ± 1	371 ± 2
AM annealed at 820 °C	758 ± 7	943 ± 3	23 ± 0	330 ± 1
AM annealed at 940 °C	729 ± 9	929 ± 5	22 ± 1	318 ± 3
Vaco as-delivered	864 ± 8	941 ± 4	22 ± 0	318 ± 1

ultimate tensile strength of 955 MPa and hardness 370 HV10, and had a high yield strength of 815 MPa, combined with the lowest total elongation of 19%. Post-process solution annealing at 820 °C caused yield strength to drop to 758 MPa and led to a slight decrease in tensile strength to 943 MPa and to an increase in total elongation to 23%. Post-process solution annealing of AM steel at a higher temperature of 940 °C resulted in the lowest yield strength of 729 MPa and tensile strength of 929 MPa with 22% elongation. Finally, the conventionally manufactured Vaco steel was tested in as-delivered (i.e. solution annealed) condition, showing a yield strength of 864 MPa, tensile strength of 941 MPa and 22% elongation.

The hardness of the AM steel generally decreased upon solution annealing. The solution annealing at the higher temperature produced lower hardness, 318 HV10, which was equal to the hardness of conventionally manufactured Vaco.

3.3.2. *Tensile test of hardened samples*

Yield and ultimate tensile strengths in all the materials increased as the precipitation hardening temperature was raised from 250 °C to 500 °C (Fig. 12, Fig. 13). In addition, at each of these hardening temperatures, the strength increased with holding time from 0 to 6 h. Both of these effects are caused by an increasing number of precipitates appearing in the microstructure. The development of mechanical properties strongly suggests that the changes in the microstructures must have happened already at the temperature 350 °C. It was mentioned in the microscopy section that precipitation is generally observed in SEM micrographs of AM maraging steel hardened at temperatures around 400 °C and higher. However, the early stages of the precipitation process, which are not traceable in SEM micrographs, could contribute to the strengthening of the steel, such as the formation of nanoprecipitates documented by HRTEM observation in Ref. [4]. The rather sharp increase of strength and hardness for all hold times at 350 °C would imply that precipitation hardening actually happens at lower temperatures than generally expected and even after relatively short exposures. At the highest hardening temperature of 550 °C, all the materials exhibited a new kind of behaviour: their strengths decreased with increasing time and the drop of strength was more significant for longer times at that temperature. This abrupt change in mechanical properties could be attributed to the competing effect of two-phase transformations. The effect of precipitation hardening, which strengthened the material at lower hardening temperatures, is diminished at 550 °C and outweighed by the onset of austenite reversion. A significant increase in austenite volume fraction after the 6-h hardening at 500 °C and a further increase after the 6-h hardening at 550 °C was confirmed by metallographic observation and X-ray diffraction (Figs. 10 and 11). The correlation can be seen between the higher austenite fraction and decline of strength after hardening at 550 °C. The highest amount of austenite was detected in an as-built sample, which also suffered the most significant drop of yield and tensile strength and hardness.

As-built samples had the highest yield and ultimate tensile strengths at room temperature and remained so after hardening at lower temperatures. With yield strength, this ceased to apply at 400 °C, and with the tensile strength at 300 °C, regardless of the annealing times. This is connected with high heating and cooling rates applied to the steel during AM, resulting in very fine cellular microstructure with high residual stresses. On the other hand, these microstructures also had the lowest total elongations (Fig. 14) in the as-built condition and also after hardening at lower temperatures up to 500 °C. Their elongation values only drew closer to those of conventionally manufactured Vaco and solution-annealed AM samples after longer precipitation hardening at 550 °C. At this temperature, the increased amount of reversed austenite

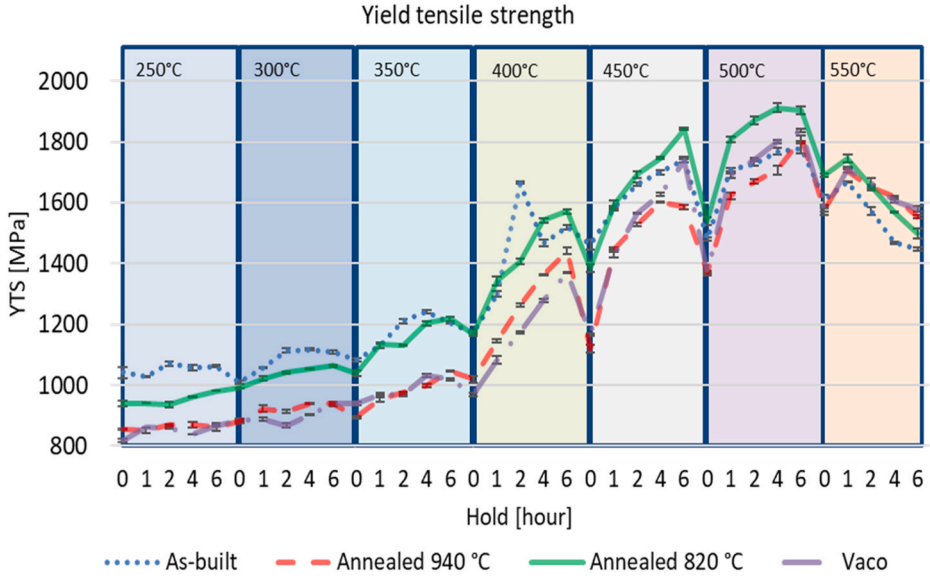

Fig. 12. Yield strength as a function of precipitation hardening temperature and time.

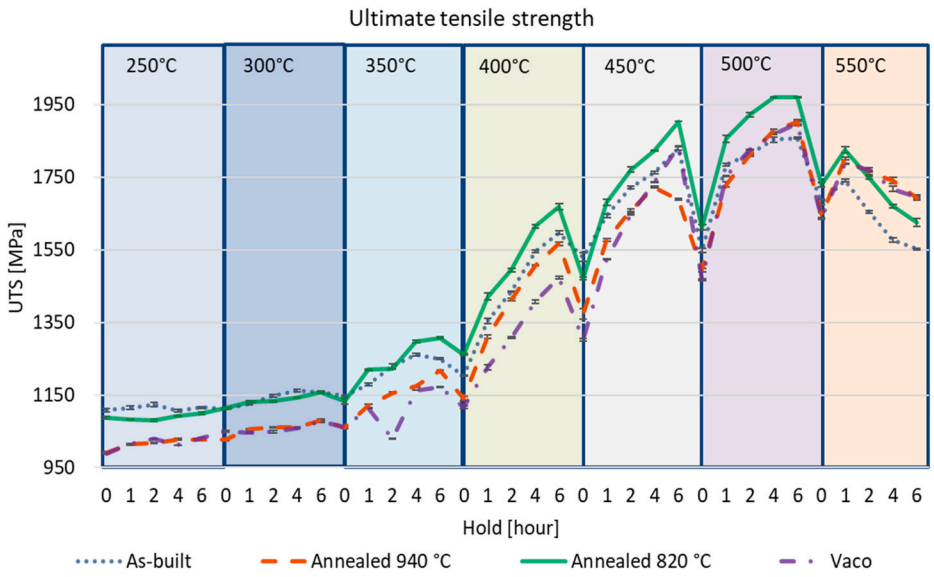

Fig. 13. Ultimate tensile strength as a function of precipitation hardening temperature and time.

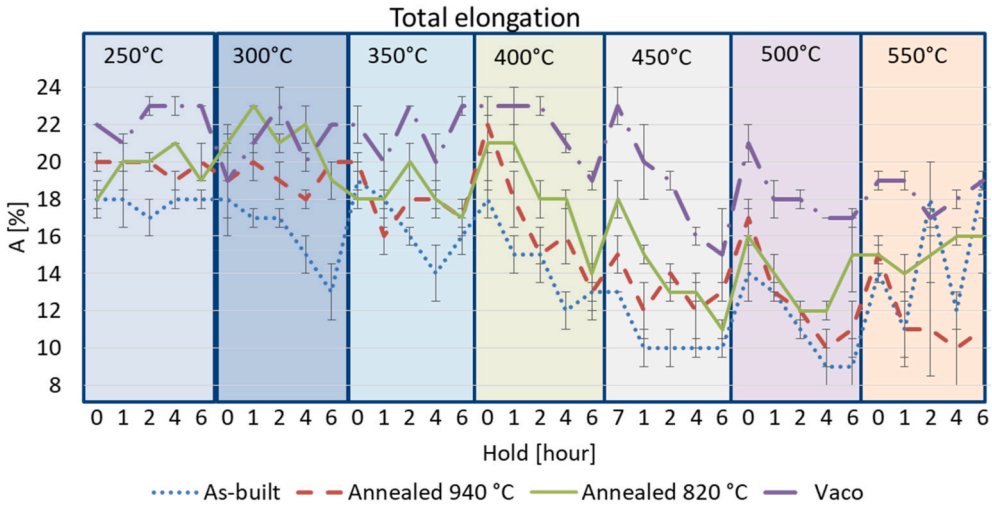

Fig. 14. Total elongation as the function of precipitation hardening temperature and time.

makes up for the lower ductility of the matrix.

Starting with 4 h at 400 °C, AM samples solution-annealed at 820 °C became those with the highest yield strength. Beyond 4 h at 350 °C, they also had the highest ultimate tensile strengths from all the samples. This can be caused by the growth of high angle boundaries grains of the matrix in as-built AM steel even at mild hardening temperatures (Fig. 7 b), while the matrix of AM samples solution-annealed at 820 °C remained distinctly finer (Fig. 9 f). This would bring the additional contribution of grain-size strengthening to the total strength and hardness of the AM samples solution-annealed at 820 °C in comparison to other conditions, where only precipitation strengthening would be in operation. Their total elongation was lower than in Vaco, higher than in the as-built samples and comparable to the AM samples solution-annealed at 940 °C with the same post-process heat treatment. At the highest precipitation hardening temperature of 550 °C, their behaviour followed closely the behaviour of the as-built samples, with a rather sharp decline in strengths and a smaller increase in elongation. As mentioned above, the increasing fraction of reversed austenite started to affect mechanical properties significantly at this temperature and the AM samples solution-annealed at 820 °C possessed the second highest volume fraction of austenite after the as-built samples.

The similarities in the microstructural development of as-built and AM 820 °C samples on the one hand and AM 940 °C and Vaco samples on the other hand, were also reflected in the development of their mechanical properties during precipitation hardening. As-built samples and AM samples solution-annealed at 820 °C showed similar trends in yield strength and tensile strength with increasing hardening temperature and annealing time (blue and green curves in Figs. 12 and 13), whereas AM samples pre-annealed at 940 °C had yield and tensile strengths similar to conventionally manufactured Vaco (violet and red curves in Figs. 12 and 13).

It is interesting to note that ultimate tensile strength and yield strength increased steadily with increasing hardening temperature up to 550 °C, even for those samples which were only brought to but not held at temperature ("0 h") (Fig. 15).

This trend is seen in Vaco and the samples solution-annealed at 940 °C as early as at 300 °C. This would imply that the subtle microstructure changes responsible for the strengthening of the steel started to happen rather quickly at those low temperatures. In as-built samples and samples annealed at 820 °C, this began to show from a temperature of 350 °C. Samples which were precipitation-hardened for 6 h also showed an increase in strength with increasing hardening temperature. This,

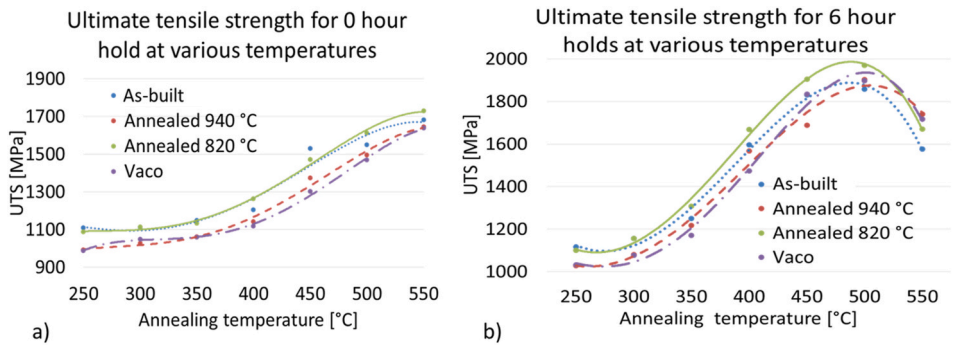

Fig. 15. Development of tensile strength with increasing hardening temperature. a) For samples with 0 annealing time (cooled immediately after reaching the desired temperature) and b) with the longest, 6-h annealing time.

however, only applied up to 500 °C. At this temperature, maximum tensile strengths were reached for all four materials after a 6-h hold. Hardening at 550 °C then produced significantly lower tensile strengths due to an increased fraction of reversed austenite.

Another measure often used for the evaluation of mechanical properties of high strength steel is the product of ultimate tensile strength and total elongation (UTSxTE, Fig. 16). This value is often seen as a measure of the toughness of the material and it is therefore used to compare the performance of steels with varying chemical composition or samples processed by various heat or thermo-mechanical treatments. It should be noted that for the materials with similar strengths, the smallest differences in total elongation can markedly influence the value of the UTSxTE product. The highest product of tensile strength and elongation was in the initial condition obtained for the AM steel annealed at 820 °C (21689 MPa%), followed closely by conventionally produced VACO 180 steel (20702 MPa%). A similar trend can be seen for all heat treatment conditions, where those two materials keep at the top of the graph. Apparently, at lower hardening temperatures (till 400 °C), up to the 6 h hold, both materials reached more or less equivalent products of UTSxTE. On the other hand, higher hardening temperatures already resulted in the further increase of the UTSxTE product for the conventionally produced steel, while the product of the AM steel pre-annealed at 820 °C slightly decreased. This difference was caused by better total elongation of the conventionally produced steel. Even though the AM steel pre-annealed at 820 °C obtained the highest tensile strength at the hardening temperatures of 400–500 °C, it was handicapped by lower elongation. The high values of the UTSxTE product of the conventionally produced steels were matched only in the over-aged stage after long holds at 550 °C by samples of AM as-built steel. At this stage, the highest volume fractions of austenite in AM as-built samples contributed to a significant increase of total elongation which was in turn mainly responsible for the sudden leap of UTSxTE product.

4. Discussion

Additively manufactured samples in an as-built condition possessed a very fine cellular microstructure. Besides the simple and rather coarse Fe or Ti oxides, which could be considered as metallurgical defects or inclusions of AM steel, three other types of much finer particles were found in the microstructure. Occasionally, very fine Ti, Al and O containing spherical particles with the diameter typically around 40 nm were observed. Even finer particles with increased Ti content were also visible in the as-built microstructure; however, it was impossible to determine their chemical composition by EDS. They might have been extremely fine Ni_3Ti precipitates or Ti oxides. The third type of particles were sharp-edged particles with increased Al, Ti and N contents. This combination of particles was not mentioned previously in the reports of AM steel, even though various research groups published their descriptions of the as-built microstructure of the AM 1.2709 maraging steel.

Researchers generally agree that fine Ni_3Ti precipitates can emerge during the AM process [4,19,35] due to the intrinsic heat treatment taking place during AM, as layers in the build are repeatedly reheated during the deposition of subsequent layers [4]. It should be noted, however, that some researchers did not observe any precipitation in as-built maraging steel [6,33,36] and therefore, they concluded that intrinsic heat treatment didn't induce precipitation during the building process. In some of these works, very fine Ti oxides with 80–180 nm diameter were reported in as-built maraging steels [6]. This confusion might be caused by slight variations in the process parameters used by

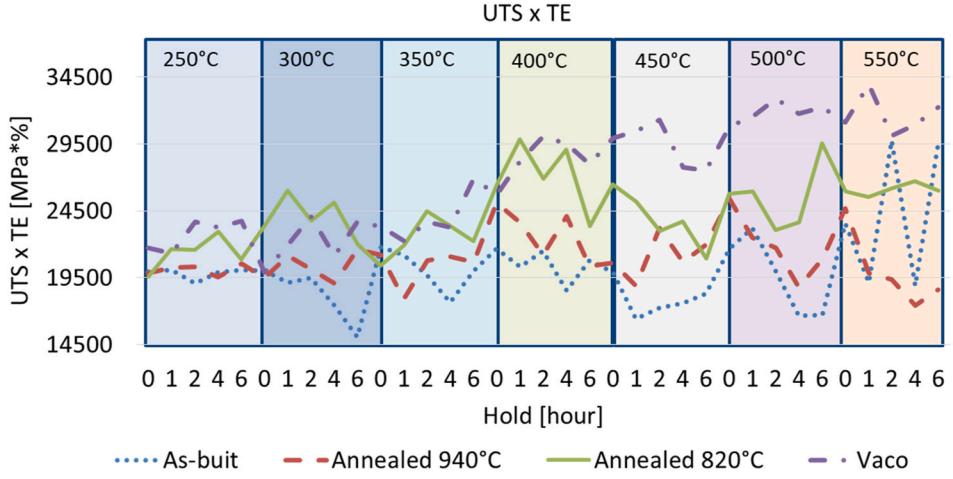

Fig. 16. Product of ultimate tensile strength and total elongation as the function of precipitation hardening temperature and time.

each research team [36], but also by the difficulties in characterizing the fine particles or 5–20 nm sized nanoparticles described by Tan et al. [4]. Although conventional EDS can detect locally increased Ti levels at least in larger particles, it is difficult to determine whether this is due to Ni_3Ti particles, a Ti-based oxide or a very fine grain of retained austenite with an increased content of alloying elements – or indeed a combination of all or some of the above in close proximity.

Mechanical properties of the four initial states of the steel reflect their microstructures. The highest strength and hardness of the as-built AM steel is generally ascribed to its very fine cellular microstructure, retained residual stress and higher dislocation density [7]. The stress is relieved during the post-processing solution annealing which results in a decrease of strength and hardness and in an improvement of elongation. Another important factor affecting the mechanical properties is recrystallization which can occur during the solution annealing. Depending on the chosen annealing temperature and hold, recrystallization might be accompanied with coarsening of the newly formed grains. Slight differences in mechanical properties of samples annealed at two different temperatures 820 °C and 940 °C can be related to a various degree of recrystallization and grain growth of AM steel reflected in their microstructures. Annealing at the lower temperature of 820 °C produced rather a fine microstructure of the matrix which achieved higher strengths and hardness than a coarser microstructure obtained by annealing at the higher temperature of 940 °C. The shorter 60-min hold at 820 °C clearly promoted recrystallization but was too short for subsequent grain growth to occur in contrast to the hold at the same temperature described in Ref. [33]. The significant grain growth was therefore observed only after solution annealing at the higher temperature of 940 °C. The elongation of the AM steel was improved by solution annealing at both temperatures, due to the decrease in dislocation density provided during the recrystallization process.

Development of the mechanical properties of the steel with increasing temperature of the precipitation hardening can be related to the microstructures of the treated samples. Generally, most of the previous works concentrated on the hardening temperatures of 400–550 °C where the strengthening of the steel is already undisputable. It can be, however, seen from the comparison of Table 3 with Figs. 12 and 13 that yield and ultimate tensile strengths already increase after annealing at the lowest temperature of 250 °C and gradually further increased with increasing annealing temperature of 300 °C. This increase is only getting more pronounced for all the samples annealed at 350 °C and really very steep for samples treated at 400 °C. This trend is best seen in samples pre-annealed at 820 °C where the yield strength increased from 758 MPa in an initial state to 940 MPa after 250 °C/2 h to 1040 MPa after 300 °C/2 h, 1132 MPa at 350 °C/2 h and 1400 MPa after 400 °C/2 h annealing. This means that even after only 2-h exposure at 350 °C, the yield strength of the steel pre-annealed at 820 °C increased by a half. The same trend is followed also by the ultimate tensile strengths. The strengthening reached a peak for all four initial conditions at 5–6 h annealing at 500 °C which was followed by a drop at 550 °C where an over-aging already occurred. Mechanical properties of all the initial conditions follow the same trend, however the highest strengths are connected with the 6 h hold at 350 °C reached by samples pre-annealed at 820 °C.

Based on the detailed atom probe tomography studies, it was concluded [7] that no significant differences between the size, density, chemical composition and morphology of precipitates were observed at peak hardening (480 °C/6 h) between precipitation hardened AM maraging steel and conventionally produced annealed and hardened maraging steel. Differential scanning analysis further suggested that the aging sequences should be equivalent for AM precipitation-hardened steel and AM solution-annealed steel hardened at the same conditions [34]. This would explain why the properties of all four initial states follow closely the same trends in Figs. 12, Fig. 13, Fig. 14. It also implies that differences in mechanical properties observed between various initial conditions should be caused mainly by other microstructure features, such as the grain size of the matrix and volume fraction and distribution of reversed austenite. Those factors really differ for various initial states, as can be seen clearly from Figs. 9 and 11. Generally, the samples with finer grain size are as-built and pre-annealed at 820 °C and they also possess higher yield and tensile strengths for all precipitation temperatures than AM samples pre-annealed at 940 °C and conventionally prepared VACO 180 with the distinctively coarser microstructure of the matrix (Fig. 9). It is also apparent from the comparison of Fig. 9b and e that the grain size of the matrix of AM as-built steel started to outgrow the AM samples pre-annealed at 820 °C after 6 h hardening at 250 °C. This might explain why the strength of the AM samples pre-annealed at 820 °C equalled and then slightly surpassed that of AM as-built samples at higher hardening temperatures. This advantage of the finest microstructure of the lattice becomes the most visible at the peak hardening temperature of 500 °C where the samples pre-annealed at 820 °C developed by far the finest, lath microstructure. Intensive reversion of austenite at the hardening temperature of 550 °C affected strongly the mechanical properties of the over-aged samples. At the short hold times (0 and 1 h) where only several presents of reversed austenite were transformed (Fig. 11), the finest microstructure of AM samples pre-annealed at 820 °C still holds the highest yield and ultimate tensile strengths. Longer holds enabled more reversed austenite to form, particularly in AM as-built and AM samples pre-annealed at 820 °C (Fig. 11). Despite their finer microstructure (Fig. 9), the strengths of those two samples started to fall more rapidly than the strengths of AM sample pre-annealed at 940 °C and conventionally prepared VACO 180 which possessed the lowest volume fractions of reversed austenite (Fig. 11).

The precipitation sequence of 1.2709 maraging steel described by various authors could be used to explain the same trend in the development of mechanical properties of all four initial conditions. It consists of the formation of μ-, S- and X-intermetallic phases at lower precipitation temperatures [14,28] followed by increasing numbers of Ni_3Ti precipitates which became rather intensive at 400 °C. This is the reason why all four conditions showed a remarkable increase of strength after the precipitation hardening at 400 °C and also the decline of elongation which is visible for all four conditions from this hardening temperature (Fig. 14). At longer holds at 400 °C and higher hardening temperatures, the original precipitates coarsened and at the same time, the new A_3B particles grew with the possible substation of Ti by Mo or Al, resulting in a further significant increase in strengths of all four conditions. Those lately appearing A_3B particles can have a distinctive rod or needle-like shape and can possess a preferential orientation, which was described by Refs. [6,7]. At the highest precipitation temperature of 550 °C, the over-aging results in the transformation of the meta-stable Ni_3Mo particles to the equilibrium Fe_2Mo phase [4] or Fe_7Mo_6 phase [34]. This process is accompanied by a local increase of Ni content in the surrounding matrix which supports the intensive austenite reversion in those areas [14,28] and results in the drop in strengths. Apparently for all used hardening temperatures, shorter holds at the temperature mean less precipitation and therefore lower strengthening effect.

Mechanical properties of the AM steel can be affected not only by the microstructure of the steel but also by the presence of printing defects. Besides Ti or Fe oxide inclusions, porosity is another defect typically found in the AM maraging steel. Generally, the degree of porosity can be influenced by the choice of printing parameters (such as laser power and laser scanning rate, etc.). Another verified way of porosity management is post-processing treatment by HIP (high isostatic pressure) processing. Recently, the high-temperature annealing treatment has been suggested to decrease the porosity of the AM steels [37]. However, the work doesn't provide enough information for the discussion of the reliability of the obtained results. When the comparative measurement was carried out on a single AM sample divided into two parts, the porosity of a solution-annealed half was slightly higher than the porosity of the un-treated, as-built, half of the sample (Chapter 3.2.4. Porosity). The measurement also showed that the porosity could significantly vary

within a single printed part. This observation highlights the importance of repeated measurements from various parts of the sample (not only more images from a particular cross-section) for the reliable evaluation of the porosity of AM samples by metallographic and image analysis.

5. Conclusions

The effect of precipitation hardening on the microstructure and mechanical properties of maraging steel was investigated in a temperature interval of 250 °C–550 °C. For this purpose, the same precipitation hardening heat treatment was applied to maraging steel prepared in four different initial conditions. These conditions were as follows: additively manufactured (selective laser melted) as-built condition, additively manufactured and solution annealed at 820 °C, additively manufactured and solution annealed at 940 °C, and conventionally manufactured steel under the Vaco brand name in the solution-annealed condition.

The initial condition of the material affected the microstructure and mechanical properties obtained by precipitation hardening, even for low hardening temperatures of 250–300 °C. In comparison, the as-built steel had similar microstructure and properties to additively manufactured steel solution annealed at 820 °C, as the lower annealing temperature resulted also in a fine-grained microstructure. On the other hand, additively manufactured steel solution annealed at 940 °C possessed similar microstructure and mechanical properties to conventionally manufactured Vaco. Due to the recrystallization and subsequent grain growth in the matrix annealed at a higher temperature of 940 °C, a coarser grain size similar to that of conventional Vaco was obtained.

The strengths of all four materials increased with increasing precipitation hardening temperatures and times up to 500 °C, where the highest strengths in the region of 1720–1960 MPa were reached. Overageing then occurred upon hardening at 550 °C. A significant amount of austenite (13–32%) formed and led to reduced strengths, particularly in the AM steel and AM steel solution-annealed at 820 °C. Slight strengthening of the steel started to be visible for all initial conditions already after the 6 h hardening at 300 °C and significant strengthening was observed from 4 h hardening at 350 °C, suggesting an early stage of precipitation process might already occur after 6-h exposure at those temperatures.

As-built samples had the highest strengths of all the initial samples and remained so after the short-time and low-temperature precipitation hardening routes. This was caused by a combination of a very fine cellular microstructure and high residual stresses in AM samples. The ultimate tensile strength of AM steel solution-annealed at 820 °C became higher starting with the hardening temperature of 350 °C. At this temperature, the matrix of the AM steel became already coarser than in the AM steel solution-annealed at 820 °C. Regarding the yield strength, the increasing strength began from 400 °C when more significant precipitation was observed. The strengths of AM pre-annealed at 820 °C were surpassed by Vaco and AM pre-annealed at 940 °C only after longer times at 550 °C. This more distinctive decline of the strength of the overaged AM samples pre-annealed at 820 °C was connected with a much higher amount of revered austenite (23%).

Data availability

The raw/processed data required to reproduce these findings cannot be shared at this time as the data also forms part of an ongoing study.

CRediT authorship contribution statement

Ludmila Kučerová: Conceptualization, Methodology, Writing – original draft, Writing – review & editing, Validation, Visualization, Supervision. **Karolina Burdová:** Investigation, Writing – review & editing. **Štěpán Jeníček:** Conceptualization, Methodology, Resources, Investigation. **Iveta Chena:** Investigation, Writing – review & editing.

Declaration of competing interest

The authors declare that they have no known competing financial interests or personal relationships that could have appeared to influence the work reported in this paper.

Acknowledgement

The present contribution has been prepared under project ITI CZ.02.1.01/0.0/0.0/18_069/0010040, “Research of additive technologies for future application in mechanical engineering practice – RTI plus” under the auspices of the National Sustainability Programme I of the Ministry of Education of the Czech Republic aimed to support research, experimental development and innovation.

References

[1] R.F. Decker, J.T. Eash, A.J. Goldman, 18% nickel-maraging steel, Trans. ASM 55 (1962) 58.
[2] Y. He, K. Yang, W. Sha, Microstructure and mechanical properties of a 2000 MPa grade Co-free Maraging Steel, Metall. Mater. Trans. 36 (2005) 2273–2287, https://doi.org/10.1007/s11661-005-0100-9.
[3] E. Jägle, Z. Sheng, P. Kürnsteiner, S. Ocylok, A. Weisheit, D. Raabe, Comparison of maraging steel micro- and nanostructure produced conventionally and by laser additive manufacturing, Materials 10 (2017) 1–15, https://doi.org/10.3390/ma10010008.
[4] C. Tan, K. Zhou, W. Ma, P. Zhang, M. Liu, T. Kuang, Microstructural evolution, nanoprecipitation behavior and mechanical properties of selective laser melted high-performance grade 300 maraging steel, Mater. Des. 134 (2017) 23–34, https://doi.org/10.1016/j.matdes.2017.08.026.
[5] H. Leitner, M. Schober, R. Schnitzer, Splitting phenomenon in the precipitation evolution in an Fe–Ni–Al–Ti–Cr stainless steel, Acta Mater. 58 (2010) 1261–1269, https://doi.org/10.1016/j.actamat.2009.10.030.
[6] E.A. Jägle, P.-P. Choi, J. Van Humbeeck, D. Raabe, Precipitation and austenite reversion behavior of a maraging steel produced by selective laser melting, J. Mater. Res. 29 (2014) 2072–2079, https://doi.org/10.1557/jmr.2014.204.
[7] E.A. Jägle, Z. Sheng, L. Wu, L. Lu, J. Risse, A. Weisheit, D. Raabe, Precipitation reactions in age-hardenable alloys during laser additive manufacturing, J. Occup. Med. 68 (2016) 943–949, https://doi.org/10.1007/s11837-015-1764-2.
[8] S.-J. Kim, C.M. Wayman, Strengthening behaviour and embrittlement phenomena in Fe-Ni-Mn-(Ti) maraging alloys, Mater. Sci. Eng. 207 (1996) 22–29, https://doi.org/10.1016/0921-5093(95)10004-0.
[9] R.F. Decker, S. Floreen, Maraging steel—the first 30 years, in: R.K. Wilson, Maraging Steels: Recent Developments and Applications, Proceedings of the Symposium TMS Meeting, Phoenix, AZ, USA, 25–29 January 1988; TMS: Pittsburgh, PA, USA; vols. 1–38.
[10] U.K. Viswanathan, G.K. Dey, V. Sethumadhavan, Effects of austenite reversion during overageing on the mechanical properties of 18 Ni (350) maraging steel, Mater. Sci. Eng. 398 (2005) 367–372, https://doi.org/10.1016/j.msea.2005.03.074.
[11] H. Mayer, R. Schuller, M. Fitzka, D. Tran, B. Pennings, Very high cycle fatigue of nitrided 18Ni maraging steel sheet, Int. J. Fatig. 64 (2014) 140–146, https://doi.org/10.1016/j.ijfatigue.2014.02.003.
[12] C. Mitterer, F. Holler, F. Üstel, D. Heim, Application of hard coatings in aluminium die casting — soldering, erosion and thermal fatigue behaviour, Surf. Coating. Technol. 125 (2000) 233–239, https://doi.org/10.1016/S0257-8972(99)00557-5.
[13] R. Shivpuri, S.L. Semiatin, Friction and wear of dies and die materials, in: Friction, Lubrication and Wear Technology, vol. 18, ASM Handbook—Friction, Lubrication, 1992, pp. 621–648. ASM International.
[14] S. Yin, C. Chen, X. Yan, X. Feng, R. Jenkins, P. O'Reilly, M. Liu, H. Li, R. Lupoi, The influence of aging temperature and aging time on the mechanical and tribological properties of selective laser melted maraging 18Ni-300 steel, Addit. Manuf. 22 (2018) 592–600, https://doi.org/10.1016/j.addma.2018.06.005.
[15] M. Rao, R. Gnanamoorthy, M. Kamaraj, Y. Mutoh, in: S. Senthilvelan (Ed.), Proc. Indo Japan Conf. Damage Tolerant Design and Materials, Chennai, 2004, p. 65.
[16] L. Kučerová, I. Zetková, A. Jandová, M. Bystrianský, Microstructural characterisation and in-situ straining of additive-manufactured X3NiCoMoTi 18-9-5 maraging steel, Mater. Sci. Eng. 750 (2019) 70–80, https://doi.org/10.1016/j.msea.2019.02.041.
[17] Y. He, K. Yang, W. Qu, F. Kong, G. Su, Strengthening and toughening of a 2800-MPa grade maraging steel, Mater. Lett. 56 (2002) 763–769, https://doi.org/10.1016/S0167-577X(02)00610-9.
[18] J. Mutua, S. Nakata, T. Onda, Z.-C. Chen, Optimization of selective laser melting parameters and influence of post heat treatment on microstructure and mechanical properties of maraging steel, Mater. Des. 139 (2018) 486–497, https://doi.org/10.1016/j.matdes.2017.11.042.
[19] K. Kempen, E. Yasa, L. Thijs, J.-P. Kruth, J. Van Humbeeck, Microstructure and mechanical properties of selective laser melted 18Ni-300 steel, Physics Procedia 12 (2011) 255–263, https://doi.org/10.1016/j.phpro.2011.03.033.
[20] Y. Bai, Y. Yang, D. Wang, M. Zhang, Influence mechanism of parameters process and mechanical properties evolution mechanism of maraging steel 300 by selective

laser melting, Mater. Sci. Eng. 703 (2017) 116–123, https://doi.org/10.1016/j.msea.2017.06.033.
[21] S. Floreen, The physical metallurgy of maraging steels, Met. Reviews 13 (1968) 115–128, https://doi.org/10.1179/mtlr.1968.13.1.115.
[22] R.K. Wilson (Ed.), Maraging Steels: Recent Developments and Applications, the Minerals, Metals & Materials Society, Warrendale, Pennsylvania, 1988.
[23] K. Monková, I. Zetková, L. Kučerová, M. Zetek, P. Monka, M. Daňa, Study of 3D printing direction and effects of heat treatment on mechanical properties of MS1 maraging steel, Arch. Appl. Mech. 89 (2019) 791–804, https://doi.org/10.1007/s00419-018-1389-3.
[24] S. Floreen, A.M. Bayer, in: R.K. Wilson (Ed.), Maraging Steels: Recent Developments and Applications, the Minerals, Metals & Materials Society, Warrendale, Pennsylvania, 1988, pp. 39–54.
[25] M.N. Rao, Progress in understanding the metallurgy of 18% nickel maraging steels, Int. J. Math. Res. 97 (2006) 1594–1607, https://doi.org/10.3139/146.101418.
[26] V.K. Vasudevan, S.J. Kim, C.M. Wayman, in: R.K. Wilson (Ed.), Maraging Steels: Recent Developments and Applications, the Minerals, Metals & Materials Society, Warrendale, Pennsylvania, 1988, pp. 107–123.
[27] T. Simm, L. Sun, D. Galvin, P. Hill, M. Rawson, S. Birosca, E. Gilbert, H. Bhadeshia, K. Perkins, The effect of a two-stage heat-treatment on the microstructural and mechanical properties of a maraging steel, Materials 10 (2017) 1346, https://doi.org/10.3390/ma10121346.
[28] J.M. Pardal, S.S.M. Tavares, V.F. Terra, M.R. Da Silva, D.R. Dos Santos, Modeling of precipitation hardening during the aging and overaging of 18Ni–Co–Mo–Ti maraging 300 steel, J. Alloys Compd. 393 (2005) 109–113, https://doi.org/10.1016/j.jallcom.2004.09.049.
[29] P.P. Sinha, K.T. Tharian, K. Sreekumar, K.V. Nagarajan, D.S. Sarma, Effect of aging on microstructure and mechanical properties of cobalt free 18%Ni (250 grade) maraging steel, Mater. Sci. Technol. 14 (1998) 1–9, https://doi.org/10.1179/mst.1998.14.1.1.
[30] U.K. Viswanathan, G.K. Dey, M.K. Asundi, Precipitation hardening in 350 grade maraging steel, Metall. Trans. A. 24 (1993) 2429–2442, https://doi.org/10.1007/BF02646522.
[31] L. Kučerová, I. Zetková, Š. Jeníček, K. Burdová, Hybrid parts produced by deposition of 18Ni300 maraging steel via selective laser melting on forged and heat treated advanced high strength steel, Addit. Manuf. 32 (2020) 101108, https://doi.org/10.1016/j.addma.2020.101108.
[32] S. Floreen, R.F. Decker, Heat treatment of 18% Ni maraging steel, ASM Trans. Q. 55 (1962) 518–530.
[33] F.F. Conde, J.D. Escobar, J.P. Oliveira, A.L. Jardini, W.W. Bose Filho, J.A. Avila, Austenite reversion kinetics and stability during tempering of an additively manufactured maraging 300 steel, Addit. Manuf. 29 (2019) 100804, https://doi.org/10.1016/j.addma.2019.100804.
[34] R. Casati, J. Lemke, A. Tuissi, M. Vedani, Aging behaviour and mechanical performance of 18-Ni 300 steel processed by selective laser melting, Metals 6 (2016) 218, https://doi.org/10.3390/met6090218.
[35] P. Kürnsteiner, M.B. Wilms, A. Weisheit, P. Barriobero-Vila, B. Gault, E.A. Jägle, D. Raabe, In-process precipitation during laser additive manufacturing investigated by atom probe tomography, Microsc. Microanal. 23 (2017) 694–695.
[36] S. Bodziak, K.S. Al-Rubaie, L.D. Valentina, F.H. Lafratta, E.C. Santos, A.M. Zanatta, Y. Chen, Precipitation in 300 grade maraging steel built by selective laser melting: aging at 510°C for 2 h, Mater. Char. 151 (2019) 73–83, https://doi.org/10.1016/j.matchar.2019.02.033.
[37] E. Tascioglu, Y. Karabulut, Y. Kaynak, Influence of heat treatment temperature on the microstructural, mechanical, and wear behavior of 316L stainless steel fabricated by laser powder bed additive manufacturing, Int. J. Adv. Manuf. Technol. 107 (2020) 1947–1956.